Rear interface engineering of kesterite $Cu_2ZnSnSe_4$ solar cells by adding $CuGaSe_2$ thin layers

Sergio Giraldo[1] | Robert Fonoll-Rubio[1] | Zacharie Jehl Li-Kao[1] |
Yudania Sánchez[1] | Lorenzo Calvo-Barrio[2,3] | Victor Izquierdo-Roca[1] |
Alejandro Pérez-Rodríguez[1,3] | Edgardo Saucedo[1]

[1]Catalonia Institute for Energy Research (IREC), Jardins de les Dones de Negre 1, Sant Adrià de Besòs, Barcelona, 08930, Spain

[2]Centres Científics i Tecnològics de la Universitat de Barcelona (CCiTUB), Lluís Solé i Sabarís 1-3, Barcelona, 08028, Spain

[3]IN2UB, Departament d'Enginyeria Electrònica i Biomèdica, Universitat de Barcelona, Martí i Franquès 1, Barcelona, 08028, Spain

Correspondence
Sergio Giraldo, Catalonia Institute for Energy Research (IREC), Jardins de les Dones de Negre 1, Sant Adrià de Besòs, 08930 Barcelona, Spain.
Email: sgiraldo@irec.cat

Abstract

Kesterite $Cu_2ZnSn(S,Se)_4$ thin film technology has been thoroughly investigated during the last decade as a promising solution in the field of low-cost, sustainable, and environmental-friendly photovoltaic technologies. However, despite efforts to boost kesterite solar cells performance by numerous strategies, the efficiencies remain stagnant around 13%. Some commonly observed issues in this technology refer to recombination events due to the likely presence of defects and, largely in line with the latest, the presence of voids and poor morphologies at the rear interface. This work, partly inspired by the copper indium gallium selenide (CIGS) technology and the use of wide-bandgap Ga-rich region as back surface field (BSF), focuses on an innovative approach using ultrathin CuGa layers at the rear interface to promote the formation of wide-bandgap $CuGaSe_2$, acting as an efficient electron reflector or BSF, and to function as an effective interlayer improving the kesterite crystallinity at the back interface. Kesterite $Cu_2ZnSnSe_4$ devices fabricated with added CuGa layers show a general increase in photovoltaic parameters and a significantly enhanced collection efficiency compared with reference devices without CuGa. This strategy proves to be successful, for not only passivating but also for improving the Mo/kesterite interface morphology, preventing to a large extent the presence of voids at the back region of the absorber.

KEYWORDS
back surface field (BSF), $Cu_2ZnSnSe_4$ (CZTSe), interface engineering, kesterite, thin film PV

1 | INTRODUCTION

Kesterite $Cu_2ZnSn(S,Se)_4$ (CZTSSe) is nowadays still considered one of the most promising inorganic thin film photovoltaic (PV) absorbers with a good prognostic for a large number of applications in the future, from custom-made modules with appealing features, such as flexible or colorful devices, being an ideal candidate for building- integrated PV (BIPV), to smaller modules capable of powering many types of sensors, including the wide and recent field of Internet of Things (IoT) applications.[1] In addition, kesterite holds a great number

of advantages that makes it an ideal PV semiconductor, including its environment- and sustainability-friendly features because it is synthesized from earth-abundant and low-toxicity elements, it has excellent optical absorption properties ($\alpha > 10^4$ cm^{-1}), naturally p-type conductivity, and a direct bandgap that can be easily tuned from 1.0 to 1.5 eV by simply varying the S/Se ratio,[2] and even reach higher values when cationic substitution strategies are used.[3,4]

Despite an intensive research effort in this family of semiconductor materials, the efficiency of kesterite solar cells remains stagnant at values around 13%.[5,6] Especially, comparing the certified record

device efficiency of kesterite CZTSSe (12.6%) with its more mature close cousin Cu (In,Ga)Se$_2$ (23.35%),[7] it is clear that a large improvement margin remains. It is in that context a logical approach to take inspiration from proven strategies used in copper indium gallium selenide (CIGS), specifically the rear interface engineering and the formation of a controlled cationic grading. The presence of Ga-rich CIGS at the rear interface induces a higher bandgap by mainly increasing the conduction band, thus contributing to a better collection of the charge carriers generated deeper in the absorber, which are normally associated to long-wavelength light absorption, impacting positively on the devices efficiency by increasing the current density and decreasing recombination events.[8] This concept, known as electron reflector or back surface field (BSF), has been widely exploited in many other mature PV technologies through different approaches.[9,10]

On this topic, several examples can be found in the literature for different PV materials, leading to a similar improvement of the devices performance. First, in the case of silicon solar cells, the formation of a heavily doped p-type region by using different dopant elements, like Al or B, has demonstrated an efficient BSF effect leading to a better long-wavelengths collection.[11,12] Other examples include the use of a ZnTe layer in CdTe solar cells, which can create a barrier in the conduction band due to the bandgap difference between both materials, reflecting minority carriers away from the back surface.[13] As previously mentioned, the CIGS technology relies on a Ga grading, thus forming a bandgap grading towards the back contact, and again improving the carrier collection and decreasing surface recombination at the back contact.[14] In theory, a similar approach could be applicable in the case of kesterite; however, these compositional gradients have shown to be more challenging so far.

The need of a BSF becomes relevant especially when the back surface recombination velocity begins to strongly influence solar cells performance, which is a possibility when the minority-carrier diffusion length approaches or exceeds film thickness. Moreover, the absorption coefficient of the PV material plays an important role in the aforementioned matter, as it determines the depth at which charge carriers are generated within the absorber layer. If low energy photons can create charge carriers able to diffuse towards the rear interface, an electron reflector could have a significant beneficial impact on the carriers' collection. In the case of kesterite CZTSe, although the absorption coefficient is high and the photon penetration depth is expected to remain lower than 200 nm even for low energy photons,[15,16] its diffusion length ranging from 500 nm to 2 µm[17–19] along with the typical absorber thicknesses used around 1.5 µm makes the implementation of a BSF layer a promising approach to reduce back contact recombination also in this technology.

Regarding rear interface passivation in kesterite, some strategies have been studied with relatively successful outcome. Lee et al[20] reported an effective interface passivation approach by implementing nanometer-scale Al$_2$O$_3$ thin films grown by ALD in CZTS solar cells, resulting in enhanced power conversion efficiencies by improving the V$_{OC}$, FF, long-wavelength collection efficiency, and the short-circuit current density (J$_{SC}$). Similarly, Kim et al[21] achieved remarkable V$_{OC}$ deficit improvements, suppressing nonradiative recombination via

interface passivation through patterned thin Al$_2$O$_3$ layers, applied to both front and rear interfaces. Other investigated strategies include the use of high work function MoO$_3$ layers, in which Ranjbar et al[22] demonstrated an improved minority-carrier lifetime and open-circuit voltage by introducing 10 nm of MoO$_3$ between Mo rear contact and CZTSe, showing a reduced interface recombination. Similarly, Antunez et al[23] presented a method to increase V$_{OC}$, decreasing electron-hole recombination, by using a combination of MoO$_3$ with an original Au back contact. This approach proved very useful especially for thin absorbers where the BSF effect becomes critical. On the other hand, the influence of SnS compound at the interfaces was studied by Ren et al,[24] showing promising beneficial effects for the J$_{SC}$ of the solar cells when it is located at the rear interface, likely attributable to a passivation effect.

In the same vein, the rear interface in kesterite CZTSSe has shown recurrently issues related to the presence of voids along the Mo/kesterite interface, in some cases attributed to the diffusion of the different elements during the reactive annealing and/or the formation of volatile compounds such as Sn(S,Se)$_2$.[25,26] More recently, Kim et al[27] attributed the formation of voids and secondary phases to the wettability behavior between the substrate and metal precursor, presenting promising strategies through the implementation of intermediate layers to prevent these phenomena. Besides this, there is a wide consensus on the detrimental decomposition reaction that occurs at the Mo/kesterite interface resulting in decomposition of the CZTS layer into Cu$_2$S, ZnS and SnS$_2$ and growth of MoS$_2$ (same for the selenide compound CZTSe).[28] In this regard, the implementation of several interlayers has been investigated using a variety of materials with the aim of avoiding absorber decomposition and improving the back interface morphology. López-Marino et al[29] reported a process based on the use of an ultrathin ZnO intermediate layer, inhibiting the decomposition reaction, thus leading to improved morphologies and achieving significant device performance improvements. Later on, this same strategy was further improved by applying a rapid thermal annealing (RTA) treatment on glass/Mo/ZnO substrates, where Placidi et al[30] showed greatly improved CZTSe device performance, through the increase of the shunt resistance and decreased series resistance, related to the reduction of defects induced such as voids at the back interface and cracks in the window layer. Interestingly, Schnabel et al[31] investigated on the use of TiN as interlayer, showing that direct contact between CZTSSe and Mo is necessary to form a large-grain layer near the back contact, and stating that the decomposition of the kesterite phase and formation of Mo(S,Se)$_2$ might be needed for forming large grains, although it seemed that only the presence of Mo(S,Se)$_2$ is required for achieving good performing devices. A different approach was reported by Cui et al,[32] who introduced a thin Ag intermediate layer, showing a reduction of secondary phases as well as the amount of voids, leading to better carrier collection efficiencies and lower series resistance, improving the overall performance of CZTS solar cells. In connection with the latter, recent first principle calculations showed that introducing Ag in kesterite is a promising strategy to stabilize the defect formation in the films, lowering significantly nonradiative

recombination.[33] Furthermore, the use of Al_2O_3 by the team of X. Hao was shown to be an effective method to avoid phase segregation and voids at the back contact region, achieving longer minority lifetime and reduced back contact recombination, ultimately leading to boosted CZTS solar cells efficiency.[34] On the other hand, Meng et al[35] demonstrated a carbon-doping strategy to enhance the back contact adhesion, significantly eliminating the voids with good repeatability and improved long-term stability.

In this work, partly inspired by the CIGS technology and the formation of the wide-bandgap Ga-rich rear region acting as BSF, we study the effect of adding small amounts of Ga at the back region of kesterite $Cu_2ZnSnSe_4$ (CZTSe) absorbers. The aim of this strategy is, on one hand, to promote the formation of wider bandgap $CuGaSe_2$ (CGSe) compound at the rear interface to create a BSF and, on the other hand, to investigate its impact on the interface morphology as a possible approach to prevent voids formation and improve adhesion. It is important to note that although Ga is considered a critical raw material, the quantities used in this approach are minimal; therefore, the sustainability of the presented technology would not be compromised. The method described here represents a simple yet effective strategy to address some critical limitations in kesterite CZTSe solar cells, such as the poor morphology and the presence of highly defective interfaces, increasing the likelihood of recombination events. In this context, the approach presented here shows a significant positive impact on the absorber's morphology, greatly improving the quality of the CZTSe especially at back side. The latter along with the demonstration of a BSF effect through the formation of CGSe phases, address one key issue in CZTSe technology, ultimately leading to remarkable cell performance improvements. Additional SCAPS-1D simulations are presented to study the impact of thin BSF layers as a function of the absorber thickness and discussed in regard to the experimental results.

2 | EXPERIMENTAL SECTION

Samples were prepared on Mo-coated (DC magnetron sputtering, Alliance AC450) soda-lime glass substrates. Ga addition was studied through the deposition of various thicknesses of CuGa (0, 5, 10, and 25 nm) on the Mo back contact, prior to the CZT metallic stack precursor. CuGa layers were sputtered and subsequently subjected to different preselenization treatments (samples without preselenization treatment also included). These thermal treatments were performed at temperatures ranging from 400°C to 500°C for 10 min at 1.5-mbar Ar pressure, under Se atmosphere. Then, the standard Sn/Cu/Zn metallic stack was completed on top, using optimum Cu-poor and Zn-rich composition (Cu/(Zn + Sn) ~ 0.75; Zn/Sn ~ 1.10, determined with calibrated X-ray fluorescence (XRF) (Fischerscope XVD), and subjected to reactive annealing under Se + Sn atmosphere in order to synthesize the final CZTSe absorber. The full absorber thickness was estimated at ~1.5 μm, measured by XRF and scanning electron microscopy (SEM). Ultimately, solar cell devices were fabricated by depositing 50 nm CdS by chemical bath deposition (CBD), followed by 50-nm i-ZnO and

200-nm ITO by DC-pulsed sputtering (Alliance CT100). To perform the optoelectronic characterization, 3×3 mm^2 cells were mechanically scribed using a manual microdiamond scriber (OEG Optical Metrology MR200). Further detailed experimental steps for the fabrication of CZTSe solar cell devices have been reported in previous works.[30,36]

J-V characteristics were acquired using a calibrated class AAA solar simulator (Abet Technologies). Measurements were performed at 25°C, under AM1.5G 1-sun illumination conditions (uniform illumination area of 15×15 cm^2). Spectral response measurements were carried out using a Bentham PVE300 system calibrated with Si and Ge photodiodes, to obtain the EQE of the solar cells under different bias voltage conditions. SEM was performed at 5 kV accelerating voltage using a ZEISS Series Auriga microscope. Auger spectroscopy characterization was performed in a PHI 670 Scanning Auger Nanoprobe from Physical Electronics, using a field emission electron gun working at 10 keV and 10 nA as excitation source, and scanning a surface of 15×15 μm to avoid inhomogeneities. In-depth chemical composition profiles were obtained with alternate sputtering of Ar^+ ion source(4 keV). The estimated sputter ratio was about 75 nm/min. These measurements were performed in an ultrahigh vacuum (UHV) chamber with pressures between 5×10^{-10} and 9×10^{-9} Torr in order to prevent the reabsorption of the sputtered material. The data analysis of the spectra was done with Multipak Version 9.9.08 program from ULVAC-PHI. For quantification purposes, due to very important matrix effects of the Auger measurements, sensitivity factors providedby the same program were adapted to fit actual measurements of own standard samples used as references. Raman characterization was carried out using an FHR640 and an iHR320 spectrometers (Horiba Jobin-Yvon) optimized for the 532- and 785-nm excitation wavelengths, respectively. The different penetration length in the absorber of both excitations (50-nm penetration for the 532-nm excitation, and 150-nm penetration for the 785-nm one) allowed to obtain information from points at different depth. Each spectrometer was coupled to a CCD detector cooled down to −75°C. The measurements were performed in the backscattering configuration through an Olympus objective coupled to an IREC-designed probe. Both excitations were performed using solid-state lasers. The laser power densities were kept below 220 W/cm^2 in order to prevent thermal effects. The Raman shift was calibrated by imposing the shift for the main silicon band of a Si monocrystal reference at 520 cm^{-1}. The study of the back interface was achieved by means of a mechanical lift-off, detaching the absorber from the Mo substrate. Solar cell modeling was performed using SCAPS-1D ver. 3.3.07,[37] and the model parameters were taken from various literature sources.[38,39] The model was kept as simple as possible to keep the focus on the influence of the back contact when varying the absorber thickness; the complete set of modeling parameters can be found in the supporting information.

3 | RESULTS AND DISCUSSION

As mentioned in Section 1, a consensus regarding the issues of a badly crystallized kesterite absorber in the back region exists in the

community. Usually, this includes the presence of smaller crystals, voids, in some cases segregated secondary phases, but in general, a more degraded morphology and poorer adhesion between the Mo back contact and the kesterite absorber. Figure 1 illustrates pretty well the presence of voids at the rear interface, despite the well-crystallized top layer, in a standard CZTSe reference cell (Figure 1A). Nevertheless, the implementation of a thin layer of CuGa, followed by a preselenization treatment as described in the Section 2, demonstrates a significant improvement in the rear interface morphology with a denser and well-compacted structure, showing a greatly improved adhesion between the layers. In particular, Figure 1 shows a clear improvement of the rear morphology when 25 nm of CuGa (preselenized at 400°C) are introduced before the metallic stack precursor deposition (Figure 1B). In fact, substantial improvements in the morphology are observed even for thinner layers of CuGa. Figure S1 shows the effect of only 10-nm CuGa, with and without preselenization treatment. As can be seen, when no selenization treatment is applied to the CuGa layer, although slightly bigger crystals might form, the presence of voids is not prevented. In this case, the thin CuGa layer is likely totally decomposed during the reactive annealing forming the CZTSe, leading to a slightly higher Cu amount during the annealing, which could explain the observed enlarged crystals, and to the presence of some Ga impurities in the kesterite matrix. Even though high Cu concentrations in CZTSe have been found to be detrimental for the solar cell performance, Cu-rich growth conditions are able to assist the grain growth.[40] Nonetheless, when the CuGa layer is preselenized, the morphology quality improvement is much more noticeable. In such a case, a stable thin CuGaSe$_2$ layer is expected to form, thus creating a seed layer for the kesterite growth avoiding the direct contact between the CZTSe and the Mo, and preventing its decomposition and the subsequent formation of voids. As can be noticed in Figure 1B, the half bottom part of the absorber is formed by smaller grains, especially near the rear interface. Indeed, this is due to the formation of the thin CuGaSe$_2$ layer during the preselenization step; however, the fact of being smaller crystals should not be an issue for the device performance provided the grain boundaries are well passivated and this layer provides a good contact.

To evaluate the impact of the back CuGa layers on the devices performance, a complete set of CZTSe absorbers synthesized on different thicknesses of CuGa with and without Se treatments was made into solar cells. Figure 2 shows a comparison of the different PV parameters of the devices included in this study. As may be seen,

samples with no preselenization treatment present the lowest efficiencies, especially with increasing CuGa thickness. In this regard, Kondrotas et al[41] studied previously the system Cu (In,Ga)Se$_2$-ZnSe and demonstrated the formation of Cu-Zn-Ga-Se phases, which might be responsible for the solubility of the thin CuGa layers without any treatment in the presence of Zn and Se during the reactive annealing, thus preventing the formation of a CuGaSe$_2$ layer at the back interface. In this case, the additional Cu amount together with Ga impurities throughout the absorber could explain the performance decrease. Nevertheless, when these thin CuGa layers are thermally treated under Se atmosphere, all of them lead to a general efficiency improvement regardless of the temperature used for the treatment. Surprisingly, thicknesses as low as 5 nm of CuGa (and up to 25-nm CuGa), previously preselenized, are already sufficient to achieve remarkable improvements in terms of device performance (+2% absolute increase in efficiency), showing a general improvement of V_{OC}, J_{SC}, and FF. In particular, the beneficial effect on the current density together with the V_{OC} improvement could be an indication that this CuGa layer is forming the CuGaSe$_2$ compound at the back region acting as back electron reflector. Furthermore, the positive effect on the FF would correlate well with the previously shown improved morphology at the interface, leading to a decreased series resistance in the devices. In the same way, the better morphology of the back side could also explain to a large extent the V_{OC} improvement, as the presence of defects and recombination centers would be notably reduced, therefore preventing a detrimental pinning of the quasi Fermi level and the consequent limitation on the cell voltage.

Figure 3 shows additional external quantum efficiency (EQE) measurements for selected devices without and with 25-nm CuGa. First, we can notice an enhanced charge carriers' collection with increasing the CuGa thickness, especially in the long-wavelengths region correlating well with the J_{SC} improvement. The complete set of measured EQEs of the different devices is displayed in Figure S2, showing the gradual collection efficiency improvement. This specific behavior is recurrently reported when BSF layers are used regardless of the PV technology, such as in silicon solar cells by introducing boron-based BSF,[11] in CIGS with the Ga-gradient,[14] or even in kesterite theoretical studies have shown how the introduction of a p-Si layer would efficiently act as BSF.[42] Intriguingly, also in Figure 3, the EQE measured under reverse bias voltage (-1 V) confirms a remarkable improvement in collection efficiency, likely related to lower recombination at the rear interface for the CuGa containing sample, which could be directly
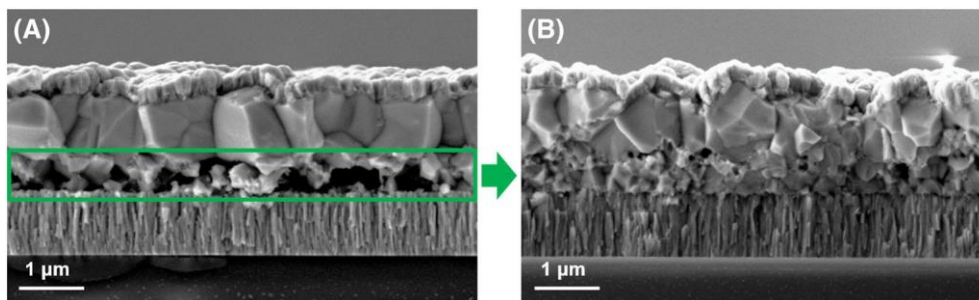

FIGURE 1   Cross-sectional scanning electron microscopy (SEM) images of a reference CZTSe cell (without CuGa) (A), and a CZTSe cell fabricated with 25-nm CuGa (preselenized) at the rear interface (B)

FIGURE 2 Photovoltaic parameters of CZTSe solar cell devices fabricated with different CuGa thicknesses added on the Mo back contact, subjected to four different treatments: no preselenization (grey), preselenization at 400°C (blue), preselenization at 450°C (purple), and preselenization at 500°C (red)
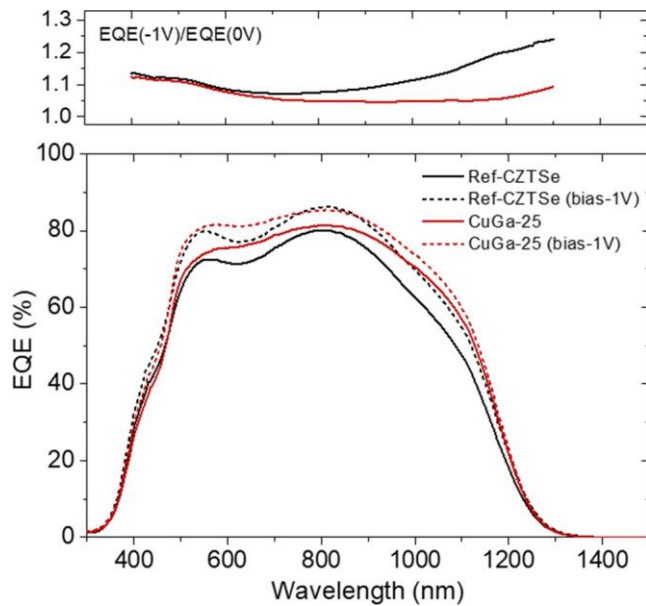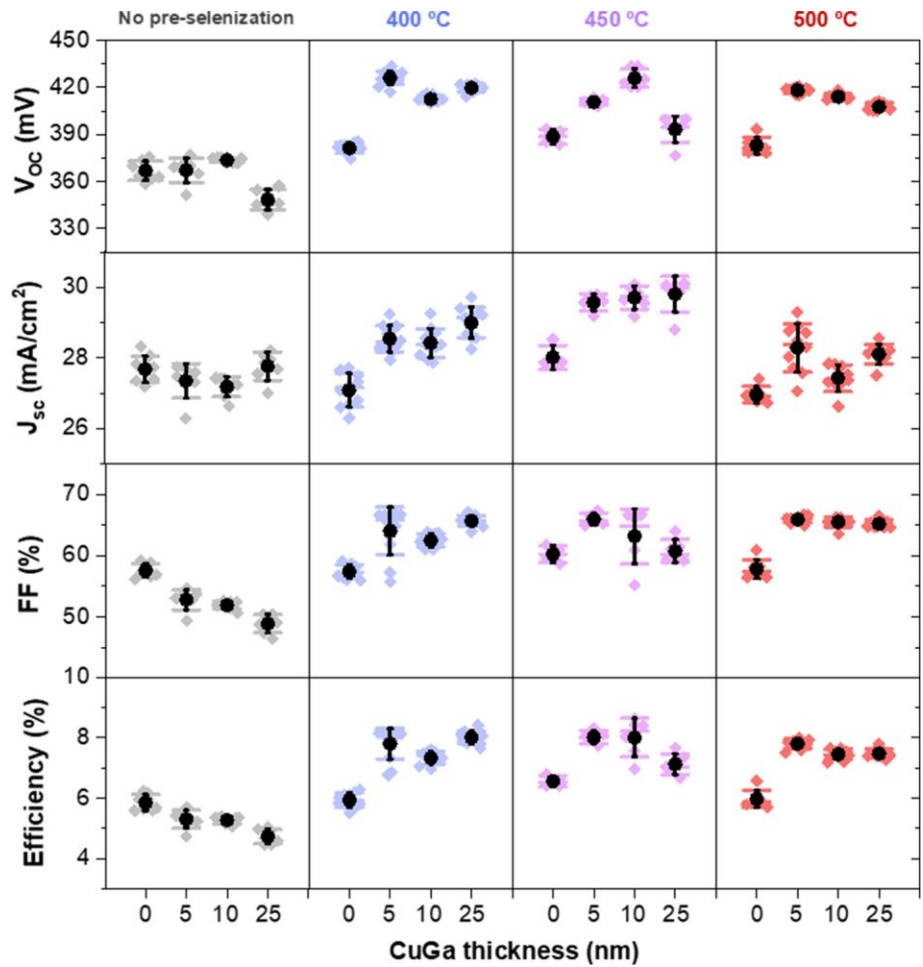

FIGURE 3 EQE spectra of a reference CZTSe solar cell device and a device fabricated with preselenized 25-nm CuGa at 400°C, measured under 0 V (solid lines) and −1 V bias voltage (dashed lines). In the upper part, the ratio EQE(−1 V)/EQE(0 V) is displayed. EQE, external quantum efficiency

associated with the observed morphology improvement as well as the fact of having a passivating layer at the back side. This is especially noted in the plot of the ratio EQE(−1 V)/EQE(0 V), displayed in the upper part of the figure.

The question of the existence of a separate $CuGSe_2$ phase however remains at this point. To have a clear answer, a combination of in-depth compositional analysis by Auger spectroscopy and detailed structural and phase analysis by Raman spectroscopy was performed on the different samples. Figure 4 shows the Auger in-depth profiling of a device fabricated with 25 nm of CuGa (preselenized) at the back side. As can be seen, especially in the zoomed view corresponding to the interface between the CZTSe and the Mo back contact, the Ga mostly accumulates at the rear interface (in the region from 12 to 20 min, sputter time). This could be a clear indication that CuGa layers, after being preselenized, are resilient enough to remain at the back interface forming most likely $CuGaSe_2$ phases. In fact, the literature about $CuGaSe_2$ thin films shows synthesis conditions very similar to the ones utilized in this work, with synthesis temperatures in the range of 530°C–550°C, which might support its stability during further cell processing.[43,44] Regarding the rest of the elements, an expected even distribution and constant flat profiles are observed, without traces of Ga in any other region of the CZTSe absorber. Additionally, Figure S3 shows a clear evolution of the Ga accumulation at
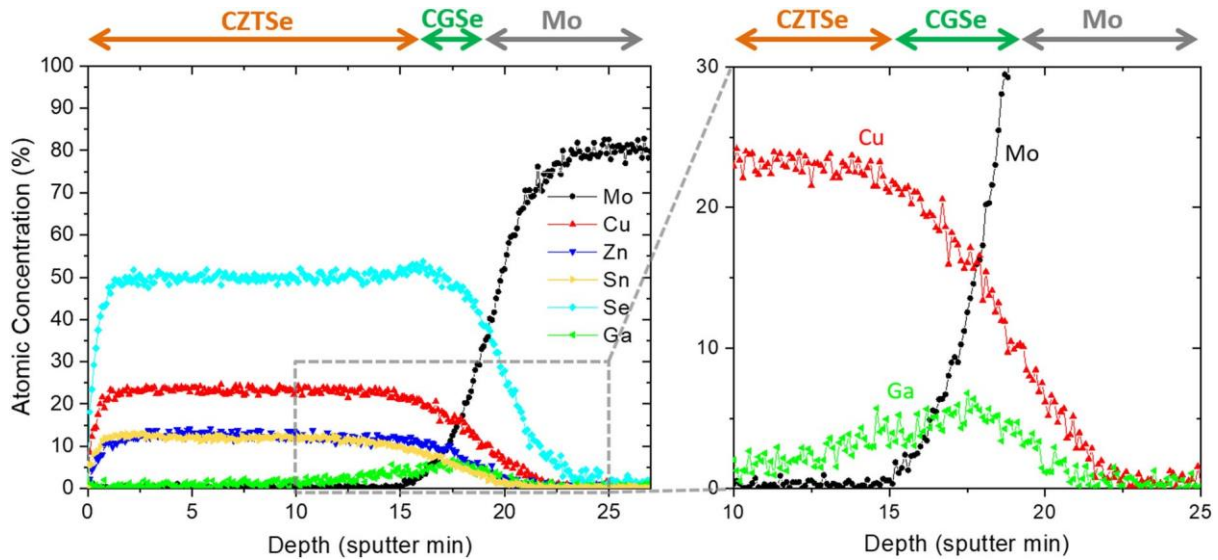
FIGURE 4 Auger spectroscopy in-depth compositional analysis of a CZTSe absorber fabricated with 25-nm CuGa (preselenized at 400°C) at the Mo/CZTSe rear interface

the back region with the increasing CuGa thickness (0, 5, 10, and 25 nm of CuGa).

Following with the same question, a deep Raman analysis with two different excitation wavelengths (532 and 785 nm) was performed on the back surface of the CZTSe absorbers, accessible through previous mechanical lift-off. Both front and back surfaces of the absorber were analyzed, as well as the remaining material on the substrate side (not shown). Figure 5 shows the Raman spectra of the back surface of the absorbers obtained for a reference CZTSe sample (without CuGa layer) and a CZTSe absorber fabricated with a 25-nm CuGa layer (CuGa-25), along with a CuGaSe$_2$ (CGSe) sample grown in

the same preselenization conditions as reference. The characteristic Raman peaks of CZTSe are observed in the reference and the CuGa-25 samples for both excitations.[45] In addition, MoSe$_2$ vibrational modes, which are enhanced with the 785-nm excitation due to resonant effects, are observed in both samples too.[46] Thus, confirming the proper formation of CZTSe at the back side, along with an expected partial selenization of the Mo back contact. It should be noted that the intensity of the peaks related to MoSe$_2$ phases can vary from one sample to another due to the nature of the mechanical lift-off process, as these phases can remain in both sides after the lift-off. In any case, the formation of thin MoSe$_2$ layers at the rear interface in
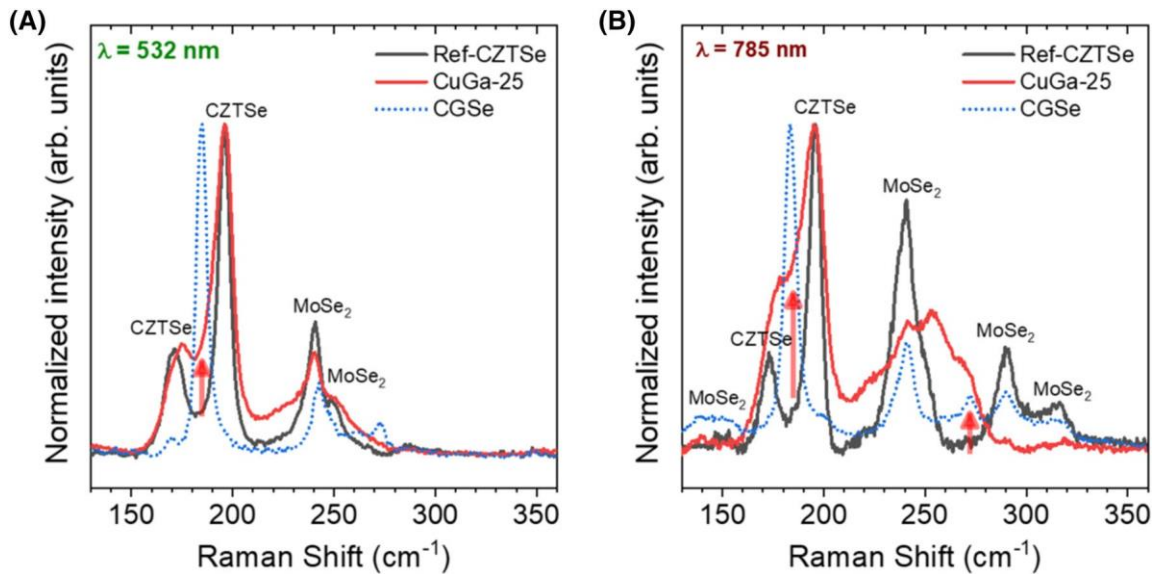

FIGURE 5 Raman analysis performed with 532- (A) and 785-nm (B) excitation wavelengths on the back surface of a reference CZTSe sample (without CuGa), a CuGa-25 sample (with 25 nm of CuGa preselenized), and a CuGaSe$_2$ sample as reference

chalcogenide solar cells has been proven to be beneficial to achieve a good ohmic contact positively affecting the device performance.[47,48] As can be noticed in the same figure, the CGSe presents a characteristic peak at 185 cm^{-1} leading to a clear contribution in the CuGa-25 spectra (measured with both excitation wavelengths). However, this is not the case in the reference CZTSe spectra, where there is only evidence of kesterite CZTSe and MoSe$_2$. An additional CGSe characteristic peak at 270 cm^{-1} leads to a clear shouldering in the CuGa-25 spectra, whereas such feature is again absent from the reference CZTSe. Regarding the front surface analysis, Figure S4 shows no significant differences between the Raman spectra of the studied samples, demonstrating the presence of the CZTSe phase, whereas no effect of the CuGa addition is observed in any absorber at the front side. These results therefore confirm the presence of resilient CGSe phases exclusively at the rear interface.

To support the experimental results presented and to discriminate between the BSF effect and the improved morphology in terms of PV performance, SCAPS-1D simulations were performed. In such model, mostly based on the Anderson approach of clear separation between layers,[49] simulating the back side morphology improvement is near impossible; implementing a BSF is however trivial. Three different scenarios were studied using three different CZTSe absorber thicknesses: (i) 1.2-μm CZTSe as the standard case (considering the size of the voids in the actual layers, this is deemed a more realistic value for the effective absorber thickness); (ii) 1.8-μm CZTSe as a thicker absorber; and (iii) 600-nm CZTSe as a thinner absorber. In all three cases, the thickness of the bottom CuGaSe$_2$ was kept constant. Figure 6 shows the effect on the PV performance for all three scenarios (Figures S5 and S6 show the SCAPS parameters used for the CZTSe and the CuGaSe$_2$ layer, respectively). As can be observed, for thick absorbers, the use of a BSF is largely irrelevant. In this case, considering the relatively low diffusion length and lifetime together with the high absorption coefficient, the absorber layer is thick enough so the vast majority of charge carriers generated (mainly within the first hundreds of nm of the CZTSe) never reach the back region; therefore, the effect of the added BSF layer proves to be negligible. However, for our standard thickness kesterite, a significant impact is observed. Here, the 1.2-μm CZTSe absorber has an optimal thickness to allow the charge carriers to diffuse toward the back interface and to be efficiently reflected by the BSF (enhancing collection) and while the absorber
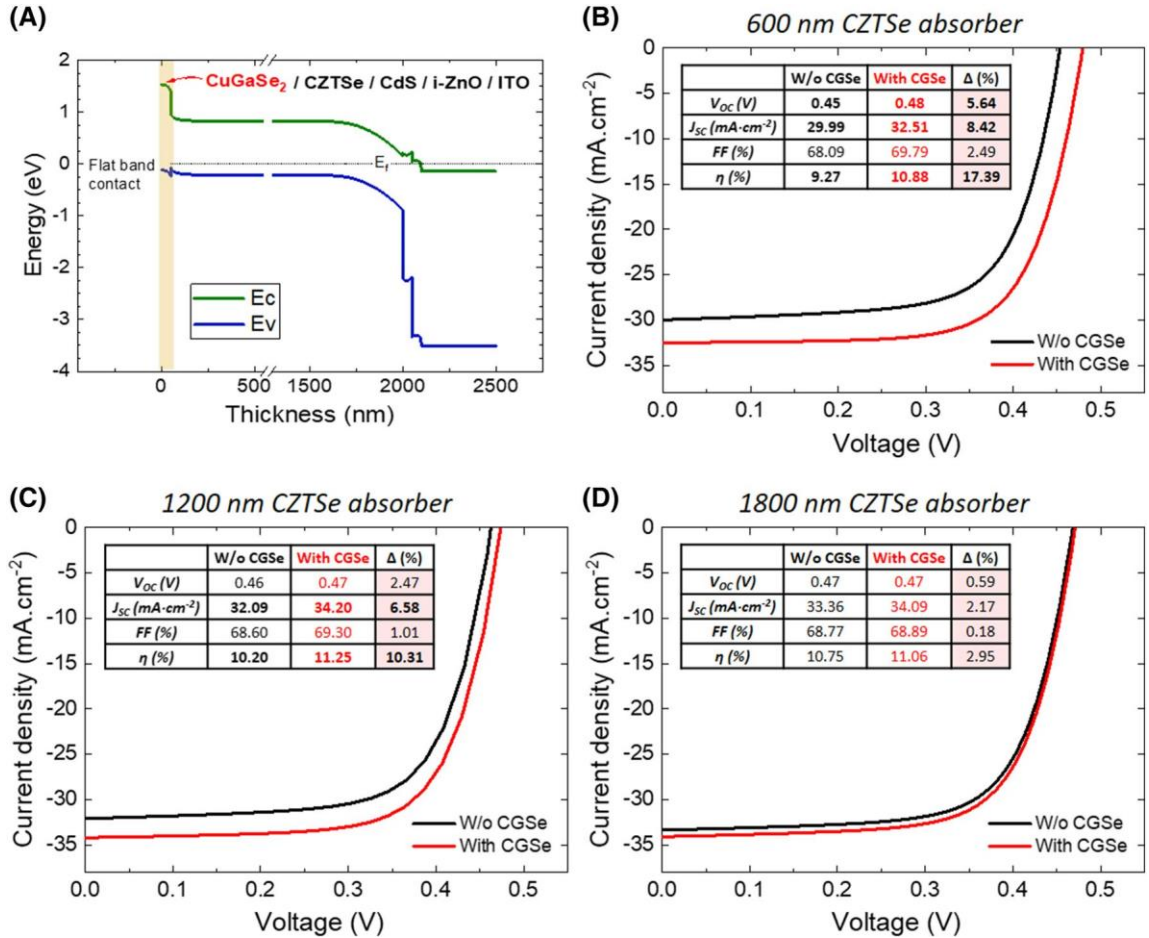

FIGURE 6 Energy band diagram of the simulated solar cell structure with CuGaSe$_2$ (A); J-V characteristics and photovoltaic parameters obtained with SCAPS-1D simulations for CZTSe solar cells with and without CuGaSe$_2$ (CGSe) at the rear interface, using different absorber thicknesses: a thinner absorber of 600 nm (B); a standard absorber of 1,200 nm (C); and a thicker absorber of 1,800 nm (D)

remains at the same time thick enough to allow for a complete photon absorption. As expected, the most remarkable improvement is the J_{SC} increase, correlating well with the previously presented experimental results. The V_{OC} also shows an improvement coming from the reduced recombination, especially when dealing with thinner absorbers, but it remains more limited than the J_{SC}. As for the FF, the improvement is only marginal regardless of the absorber thickness. It thus confirms that the FF improvement observed in the experimental part is most likely related to the better morphology of the layer and the interface than the BSF effect. Finally, taking the thinnest absorbercase (600-nm CZTSe), when the absorber thickness becomes compa- rable with that of the carrier diffusion length (460 nm using state of the art modeling parameters), and considering photon penetration depth, the $CuGaSe_2$ layer clearly preserves the PV performances by blocking back contact recombination (particularly noticeable in the J_{SC} improvement). Thus, the BSF allows for devices much more resilient to an absorber thickness reduction.

4 | CONCLUSIONS

In summary, we studied the addition of thin CuGa layers at the rear interface of kesterite CZTSe solar cells, leading to several beneficial effects. Solar cells including a CuGa precursor with thicknesses in the range of 5-25 nm show a remarkable improvement in their PV perfor- mance, provided that the CuGa is preselenized to form resilient $CuGaSe_2$ phases. Additional positive effects have been identified in the charge carrier collection especially for long wavelengths, revealing an effective passivation/BSF effect. Furthermore, this approach has been proven extremely useful to prevent the formation of voids at the back side and improve significantly the interface morphology, the $CuGaSe_2$ film acting as a seed layer for the growth of higher quality absorbers. Finally, the presence of $CuGaSe_2$ phases exclusively at the interface has been demonstrated by means of Raman spectroscopy supported by Auger depth profiles. A solar cell model using SCAPS-1D supports the experimental results presented, allowing to relate the different improvements observed to either the morphology or the BSF effect, respectively. Ultimately, this work presents an innovative strategy for facing some relevant issues in kesterite solar cells, such as the poor rear interface morphology and the lack of new promising approaches to overcome the current relatively low device efficiencies.

ORCID

Sergio Giraldo https://orcid.org/0000-0003-4881-5041
Robert Fonoll-Rubio https://orcid.org/0000-0002-6292-6648
Zacharie Jehl Li-Kao https://orcid.org/0000-0002-2610-5973
Yudania Sánchez https://orcid.org/0000-0002-5740-1150
Lorenzo Calvo-Barrio https://orcid.org/0000-0002-6993-1482
Victor Izquierdo-Roca https://orcid.org/0000-0002-5502-3133
Alejandro Pérez-Rodríguez https://orcid.org/0000-0002-3525-1497
Edgardo Saucedo https://orcid.org/0000-0003-2123-6162

REFERENCES

1. Larramona G, Choné C, Meissner D, et al. Stability, reliability, upscaling and possible technological applications of kesterite solar cells. *J Phys Energy*. 2020;2(2):024009. https://doi.org/10.1088/ 2515-7655/ab7cee
2. Mitzi DB, Gunawan O, Todorov TK, Wang K, Guha S. The path towards a high-performance solution-processed kesterite solar cell. *Sol Energy Mater sol Cells*. 2011;95(6):1421-1436. https://doi.org/10. 1016/j.solmat.2010.11.028
3. Romanyuk YE, Haass SG, Giraldo S, et al. Doping and alloying of kesterites. *J Phys Energy*. 2019;1(4):044004. https://doi.org/10.1088/ 2515-7655/ab23bc
4. Giraldo S, Jehl Z, Placidi M, Izquierdo-Roca V, Pérez-Rodríguez A, Saucedo E. Progress and perspectives of thin film kesterite photovol- taic technology: a critical review. *Adv Mater*. 2019;31(16):1806692. https://doi.org/10.1002/adma.201806692
5. Wong LH, Zakutayev A, Major JD, et al. Emerging inorganic solar cell efficiency tables (version 1). *J Phys Energy*. 2019;1(3):032001. https:// doi.org/10.1088/2515-7655/ab2338
6. Wang W, Winkler MT, Gunawan O, et al. Device characteristics of CZTSSe thin-film solar cells with 12.6% efficiency. *Adv Energy Mater*. 2014;4(7):1301465. https://doi.org/10.1002/aenm.201301465
7. Green MA, Dunlop ED, Hohl-Ebinger J, Yoshita M, Kopidakis N, Ho-Baillie AWY. Solar cell efficiency tables (version 55). *Prog Photovol- taics Res Appl*. 2020;28(1):3-15. https://doi.org/10.1002/pip.3228
8. Lundberg O, Edoff M, Stolt L. The effect of Ga-grading in CIGS thin film solar cells. *Thin Solid Films*. 2005;480-481:520-525. https://doi. org/10.1016/j.tsf.2004.11.080
9. Hsiao KJ, Sites JR. Electron reflector to enhance photovoltaic effi- ciency: application to thin-film CdTe solar cells. *Prog Photovoltaics Res Appl*. 2012;20(4):486-489. https://doi.org/10.1002/pip.1143
10. Sharbati S, Gharibshahian I, Orouji AA. Proposed suitable electron reflector layer materials for thin-film CuIn1−xGaxSe2 solar cells. *Opt Mater (Amst)*. 2018;75:216-223. https://doi.org/10.1016/j.optmat. 2017.09.032
11. Singh G, Verma A, Jeyakumar R. Fabrication of c-Si solar cells using boric acid as a spin-on dopant for back surface field. *RSC Adv*. 2014;4 (9):4225-4229. https://doi.org/10.1039/C3RA45746J
12. Kaminski A, Vandelle B, Fave A, et al. Aluminium BSF in silicon solar cells. In: *Solar Energy Materials and Solar Cells*. Vol.72 North-Holland; 2002:373-379. https://doi.org/10.1016/S0927-0248(01)00185-4
13. Khosroabadi S, Keshmiri SH. Design of a high efficiency ultrathin CdS/CdTe solar cell using back surface field and backside distributed Bragg reflector. *Opt Express*. 2014;22(S3):A921-A929. https://doi. org/10.1364/oe.22.00a921
14. Ramanujam J, Singh UP. Copper indium gallium selenide based solar cells—a review. *Energ Environ Sci*. 2017;10(6):1306-1319. https://doi. org/10.1039/C7EE00826K

15. Buffière M, Brammertz G, Oueslati S, et al. Spectral current-voltage analysis of kesterite solar cells. *J Phys D Appl Phys*. 2014;47(17): 175101. https://doi.org/10.1088/0022-3727/47/17/175101

16. Henry J, Mohanraj K, Sivakumar G. Electrical and optical properties of CZTS thin films prepared by SILAR method. *J Asian Ceramic Soc*. 2016;4(1):81-84. https://doi.org/10.1016/j.jascer.2015.12.003

17. Lee YS, Gershon T, Gunawan O, et al. $Cu_2ZnSnSe_4$ thin-film solar cells by thermal co-evaporation with 11.6% efficiency and improved minority carrier diffusion length. *Adv Energy Mater*. 2015;5(7): 1401372. https://doi.org/10.1002/aenm.201401372

18. Repins IL, Moutinho H, Choi SG, et al. Indications of short minority-carrier lifetime in kesterite solar cells. *J Appl Phys*. 2013;114(8): 084507. https://doi.org/10.1063/1.4819849

19. Gunawan O, Pae SR, Bishop DM, et al. Carrier-resolved photo hall measurement in world-record-quality perovskite and kesterite solar absorbers. February 2018. http://arxiv.org/abs/1802.07910

20. Lee YS, Gershon T, Todorov TK, et al. Atomic layer deposited aluminum oxide for interface passivation of $Cu_2ZnSn(S,Se)_4$ thin-film solar cells. *Adv Energy Mater*. 2016;6(12):1600198. https://doi.org/10.1002/aenm.201600198

21. Kim J, Park S, Ryu S, Oh J, Shin B. Improving the open-circuit voltage of $Cu_2ZnSnSe_4$ thin film solar cells via interface passivation. *Prog Photovoltaics Res Appl*. 2017;25(4):308-317. https://doi.org/10.1002/pip.2864

22. Ranjbar S, Brammertz G, Vermang B, et al. Improvement of kesterite solar cell performance by solution synthesized MoO_3 interfacial layer. *Phys Status Solidi Appl Mater Sci*. 2017;214(1):1600534. https://doi.org/10.1002/pssa.201600534

23. Antunez PD, Bishop DM, Lee YS, et al. Back contact engineering for increased performance in kesterite solar cells. *Adv Energy Mater*. 2017;7(15). https://doi.org/10.1002/aenm.201602585

24. Ren Y, Richter M, Keller J, et al. Investigation of the SnS/Cu_2ZnSnS_4 interfaces in kesterite thin-film solar cells. *ACS Energy Lett*. 2017;2(5): 976-981. https://doi.org/10.1021/acsenergylett.7b00151

25. Giraldo S, Saucedo E, Neuschitzer M, et al. How small amounts of Ge modify the formation pathways and crystallization of kesterites. *Energ Environ Sci*. 2018;11(3):582-593. https://doi.org/10.1039/c7ee02318a

26. Yan C, Sun K, Liu F, Huang J, Zhou F, Hao X. Boost Voc of pure sulfide kesterite solar cell via a double CZTS layer stacks. *Sol Energy Mater sol Cells*. 2017;160(August 2016):7-11. https://doi.org/10.1016/j.solmat.2016.09.027

27. Kim SY, Kim SH, Hong S, et al. Secondary phase formation mechanism in the Mo-back contact region during sulfo-selenization using a metal precursor: effect of wettability between a liquid metal and substrate on secondary phase formation. *ACS Appl Mater Interfaces*. 2019;11(26):23160-23167. https://doi.org/10.1021/acsami.9b03969

28. Scragg JJ, Wätjen JT, Edoff M, Ericson T, Kubart T, Platzer-Björkman C. A detrimental reaction at the molybdenum back contact in $Cu_2ZnSn(S,Se)_4$ thin-film solar cells. *J am Chem Soc*. 2012;134(47): 19330-19333. https://doi.org/10.1021/ja308862n

29. López-Marino S, Placidi M, Pérez-Tomás A, et al. Inhibiting the absorber/Mo-back contact decomposition reaction in $Cu_2ZnSnSe_4$ solar cells: the role of a ZnO intermediate nanolayer. *J Mater Chem A*. 2013;1(29):8338-8343. https://doi.org/10.1039/c3ta11419h

30. Placidi M, Espindola-Rodriguez M, Lopez-Marino S, et al. Effect of rapid thermal annealing on the Mo back contact properties for $Cu_2ZnSnSe_4$ solar cells. *J Alloys Compd*. 2016;675:158-162. https://doi.org/10.1016/j.jallcom.2016.03.043

31. Schnabel T, Ahlswede E. On the interface between kesterite absorber and Mo back contact and its impact on solution-processed thin-film solar cells. *Sol Energy Mater sol Cells*. 2017;159:290-295. https://doi.org/10.1016/j.solmat.2016.09.029

32. Cui H, Liu X, Liu F, Hao X, Song N, Yan C. Boosting Cu_2ZnSnS_4 solar cells efficiency by a thin Ag intermediate layer between absorber and back contact. *Appl Phys Lett*. 2014;104(4):041115. https://doi.org/10.1063/1.4863951

33. Kim S, Márquez JA, Unold T, Walsh A. Upper limit to the photovoltaic efficiency of imperfect crystals from first principles. *Energ Environ Sci*. 2020;13(5):1481-1491. https://doi.org/10.1039/d0ee00291g

34. Liu F, Huang J, Sun K, et al. Beyond 8% ultrathin kesterite Cu_2ZnSnS_4 solar cells by interface reaction route controlling and self-organized nanopattern at the back contact. *NPG Asia Mater*. 2017;9(7):e401-e401. https://doi.org/10.1038/am.2017.103

35. Meng L, Yao B, Li Y, et al. Significantly enhancing back contact adhesion and improving stability of $Cu_2(Zn,Cd)Sn(S,Se)_4$ solar cell by a rational carbon doping strategy. *J Alloys Compd*. 2017;710:403-408. https://doi.org/10.1016/j.jallcom.2017.03.281

36. Giraldo S, Thersleff T, Larramona G, et al. $Cu_2ZnSnSe_4$ solar cells with 10.6% efficiency through innovative absorber engineering with Ge superficial nanolayer. *Prog Photovoltaics Res Appl*. 2016;24(10):1359-1367. https://doi.org/10.1002/pip.2797

37. Burgelman M, Nollet P, Degrave S. Modelling polycrystalline semiconductor solar cells. *Thin Solid Films*. 2000;361:527-532. https://doi.org/10.1016/S0040-6090(99)00825-1

38. Adachi S. *Earth-Abundant Materials for Solar Cells: Cu2-II-IV-VI4 Semiconductors*. Chichester, UK: wiley; 2015 https://doi.org/10.1002/9781119052814

39. Hanna G, Jasenek A, Rau U, Schock HW. Influence of the Ga-content on the bulk defect densities of Cu (In,Ga)Se_2. *Thin Solid Films*. 2001; 387(1-2):71-73. https://doi.org/10.1016/S0040-6090(00)01710-7

40. Hsu W-CC, Repins I, Beall C, et al. Growth mechanisms of co-evaporated kesterite: a comparison of Cu-rich and Zn-rich composition paths. *Prog Photovoltaics Res Appl*. 2014;22(1):35-43. https://doi.org/10.1002/pip.2296

41. Kondrotas R, Oliva F, Alcobe X, et al. Double band gap gradients in sequentially processed photovoltaic absorbers from the Cu (In,Ga)Se_2-ZnSe pseudobinary system. *Prog Photovoltaics Res Appl*. 2018;26(2):135-144. https://doi.org/10.1002/pip.2958

42. Minbashi M, Omrani MK, Memarian N, Kim D-H. Comparison of theoretical and experimental results for band-gap-graded CZTSSe solar cell. *Curr Appl Phys*. 2017;17(10):1238-1243. https://doi.org/10.1016/j.cap.2017.06.003

43. Jeong AR, Shin RH, Jo W, Song M, Yoon S. Synthesis and physical properties of Cu (In,Ga)Se_2 nanoparticles and CuGaSe_2 thin-films for tandem cell photovoltaic applications. In: *Conf Rec IEEE Phot Spec Conf IEEE*; 2010:3432-3434. https://doi.org/10.1109/PVSC.2010.5614600

44. Steichen M, Larsen J, Gütay L, Siebentritt S, Dale PJ. Preparation of CuGaSe_2 absorber layers for thin film solar cells by annealing of efficiently electrodeposited Cu-Ga precursor layers from ionic liquids. *Thin Solid Films*. 2011;519(21):7254-7258. https://doi.org/10.1016/j.tsf.2011.01.135

45. Guc M, Levcenko S, Izquierdo-Roca V, Fontané X, Arushanov E, Pérez-Rodríguez A. Polarized Raman scattering analysis of $Cu_2ZnSnSe_4$ and $Cu_2ZnGeSe_4$ single crystals. *J Appl Phys*. 2013;114(19):193514. https://doi.org/10.1063/1.4830028

46. Nam D, Lee JU, Cheong H. Excitation energy dependent Raman spectrum of $MoSe_2$. *Sci Rep*. 2015;5(1):1-6. https://doi.org/10.1038/srep17113

47. Pang JB, Cai YA, He Q, et al. Preparation and characteristics of $MoSe_2$ interlayer in bifacial Cu (In,Ga)Se_2 solar cells. *Physics Procedia*. 2012; 32:372-378. https://doi.org/10.1016/j.phpro.2012.03.571

48. Lopez-Marino S, Espíndola-Rodríguez M, Sánchez Y, et al. The importance of back contact modification in $Cu_2ZnSnSe_4$ solar cells: the role of a thin MoO_2 layer. *Nano Energy*. 2016;26:708-721. https://doi.org/10.1016/j.nanoen.2016.06.034

49. Anderson RL. Germanium-gallium arsenide heterojunctions [letter to the editor]. *IBM J Res Dev*. 2010;4(3):283-287. https://doi.org/10.1147/rd.43.0283